

Ditopic Chiral Pineno-Fused 2,2':6',2''-Terpyridine: Synthesis, Self-Assembly, and Optical Properties

Fu-Jie Zhao,[†] Heng Wang,[‡] Kehuan Li,[§] Xiao-Die Wang,[†] Ning Zhang,[†] Xinju Zhu,[†]
Wenjing Zhang,[†] Ming Wang,[§] Xin-Qi Hao,^{*,†} Mao-Ping Song,^{*,†} and Xiaopeng Li^{*,‡}

[†]College of Chemistry, Zhengzhou University, Zhengzhou, Henan 450001, P. R. China

[‡]Department of Chemistry, University of South Florida, Tampa, Florida 33620, United States

[§]State Key Laboratory of Supramolecular Structure and Materials, College of Chemistry, Jilin University, Changchun, Jilin 130012, P. R. China

S Supporting Information

ABSTRACT: The syntheses of 4'-substituted chiral 2,2':6',2''-terpyridine (tpy) ligands with predetermined configurations and directionalities are rather limited in the supramolecular chemistry field. In this study, a carbazole-linked ditopic chiral ligand **L** was synthesized using 4'-bromo-substituted pineno-fused tpy **5** as the precursor. Upon complexation with Cd(NO₃)₂·4H₂O and Zn(NO₃)₂·6H₂O, two enantiomerically pure metallosupramolecules, [Cd₃L₃] and [Zn₄L₄], have been self-assembled and characterized by NMR, electrospray ionization-mass spectrometry, traveling wave ion mobility-mass spectrometry, and DOSY analysis. In addition, their optical properties are characterized by UV–vis, fluorescence, circular dichroism, and circularly polarized luminescence, suggesting an efficiency transmission and amplification of chirality from the ligand to metal center via self-assembly.

Chiral self-assembly is prevalent in nature. Inspired by fascinating chiral structures with different scales in the biological world, chemists have designed and synthesized a number of elegant chiral molecular mimics with application in enantioseparation, asymmetric catalysis, recognition and sensing, pharmaceuticals, and materials.¹ Meanwhile, coordination-driven self-assembly has recently emerged as a powerful bottom-up approach to constructing nanoscale structures with well-defined sizes, shapes, geometries, and cavities.^{2,3} However, the introduction of chiral functionalities to assemble enantiomerically pure metallosupramolecules still lagged behind because of the lack of suitable chiral bridging ligands and efficient synthetic methodologies.⁴ It is therefore highly mandatory to explore novel ligands with chirality in specific positions.

2,2':6',2''-Terpyridine (tpy) derivatives have gained much attention because of their unique photophysical and electrochemical properties.⁵ With three N-binding sites, tpy-functionalized analogues⁶ could coordinate with various metal cations to form either metallopolymers⁷ or artificial supramolecular architectures,⁸ which exhibit wide applications in catalysis,⁹ biology,¹⁰ and materials science.¹¹ Accordingly, a number of strategies, including traditional ring-assembly methods¹² and cross-coupling reactions,¹³ have been developed to access a

library of tpy ligands with variable functionalizations.^{5b,14} Since the preparation of optical active pinene-type bipyridines¹⁵ have been frequently utilized to accomplish various chiral (poly)pyridines.^{16,17} Meanwhile, the rigidity, steric hindrance, and stability of pinene substituents enabled the diastereoselective synthesis of corresponding metal complexes with potential application in enantioselective reactions¹⁸ and multifunctional materials.¹⁹ Despite the above progress, the syntheses of 4'-substituted chiral tpy ligands with predetermined configurations and directionalities are rather limited.

Over the past few years, our group has developed a series of chiral pincer metal complexes and investigated their catalytic activities.²⁰ Recently, we have also contributed to discrete supramolecular fractals using multitopic tpy ligands.²¹ As a continuation of our previous work, we herein reported the synthesis of a carbazole-linked ditopic chiral ligand **L** with a chiral "pineno"-fused 2,2':6',2''-terpyridine (ctpy) moiety, which was introduced via a key precursor, viz., 4'-bromo-substituted pineno-fused tpy **5**. As a proof of concept, such a ligand could readily undergo coordination with cadmium(II) and zinc(II) to form trimeric and tetrameric metallomacrocycles with different geometries, symmetries, and cavities (Figure 1). The chiral transmission along the macrocyclic framework has been carefully investigated via circular dichroism (CD) and circularly polarized luminescence (CPL) spectrometries. Such a study illustrates that advancement of the complexity of tpy-based supramolecules could introduce a new property into the system.

The preparation of **L** started from 4-hydroxypyridine-2,6-dicarboxylic acid, which was converted to 4-bromo-2,6-diacetylpyridine (**3**) in three steps (Figure 1a).²² A subsequent Kröhnke-type reaction of *N*-heteropyridinium salt **4** with *R*-myrtenal gave **5**. It is worth noting that, although ctpy was previously reported,²³ the 4'-bromo-substituted version remained unknown regarding synthesis. Therefore, ctpy was mainly used to form dimeric mononuclear metal complexes rather than discrete metallosupramolecules assembled by a ditopic or multitopic ctpy ligand.²³ As a proof of concept, we performed a Suzuki cross-coupling of the key brominated precursor **5** with Bpin-substituted **6** to afford ditopic ligand **L**

Received: September 4, 2019

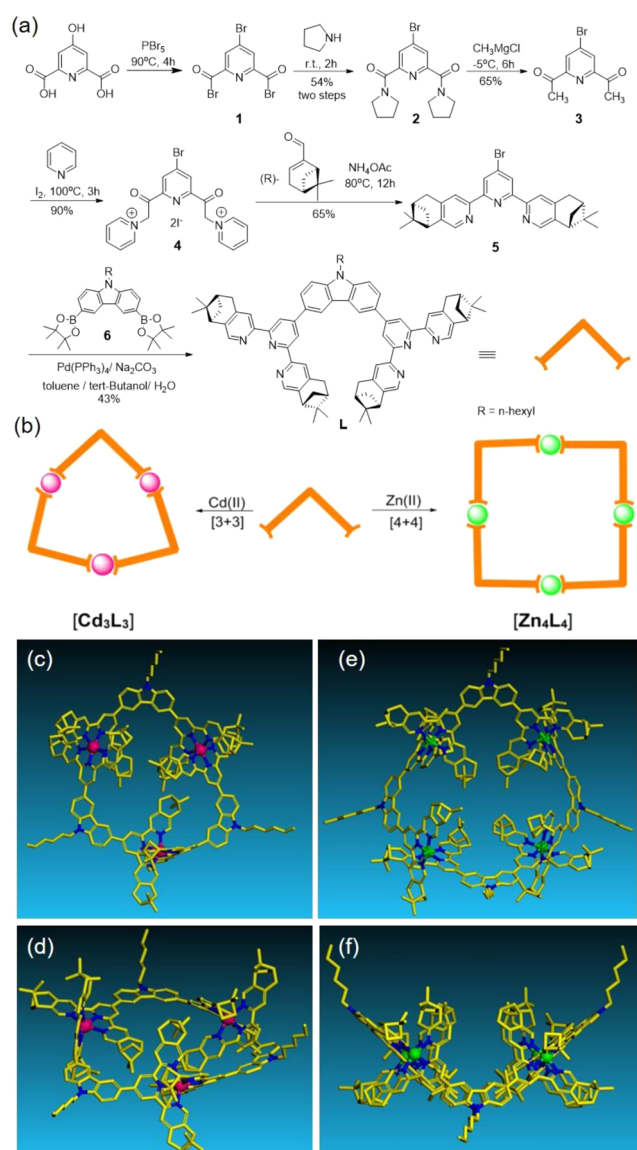


Figure 1. (a) Synthesis of L. (b) Self-assembly of $[\text{Cd}_3\text{L}_3]$ and $[\text{Zn}_4\text{L}_4]$. Energy-minimized structures from molecular modeling of trimeric $[\text{Cd}_3\text{L}_3]$: (c) top view; (d) side view. Energy-minimized structures from molecular modeling of tetrameric $[\text{Zn}_4\text{L}_4]$ macrocycles: (e) top view; (f) side view. The counterions were omitted for clarity.

in 43% yield. L was further assembled with $\text{Cd}(\text{NO}_3)_2 \cdot 4\text{H}_2\text{O}$ or $\text{Zn}(\text{NO}_3)_2 \cdot 6\text{H}_2\text{O}$, followed by treatment with excess NH_4PF_6 . Finally, metallosupramolecules with molecular compositions of $[\text{Cd}_3\text{L}_3](\text{PF}_6)_6$ ($[\text{Cd}_3\text{L}_3]$ for short) and $[\text{Zn}_4\text{L}_4](\text{PF}_6)_8$ ($[\text{Zn}_4\text{L}_4]$ for short) were obtained in 90% and 93% yields, respectively.

Figure 2 illustrates the ^1H NMR spectra of L, $[\text{Cd}_3\text{L}_3]$, and $[\text{Zn}_4\text{L}_4]$. After complexation, all of the proton signals at the A–E positions of L show obviously downfield shifts because of the decreased electron density of these protons caused by coordination with metal ions.^{8a,21} On the contrary, the proton signals at the F position are observed with an upfield shift due to the shielding effect of the metal centers.^{8a,21} More interestingly, while the $[\text{Zn}_4\text{L}_4]$ complex demonstrates a slightly broad NMR pattern in the aromatic region, the $[\text{Cd}_3\text{L}_3]$ complex exhibits a set of sharp and well-split signals corresponding to two types of ctpy signals with a 1:1 ratio (A–

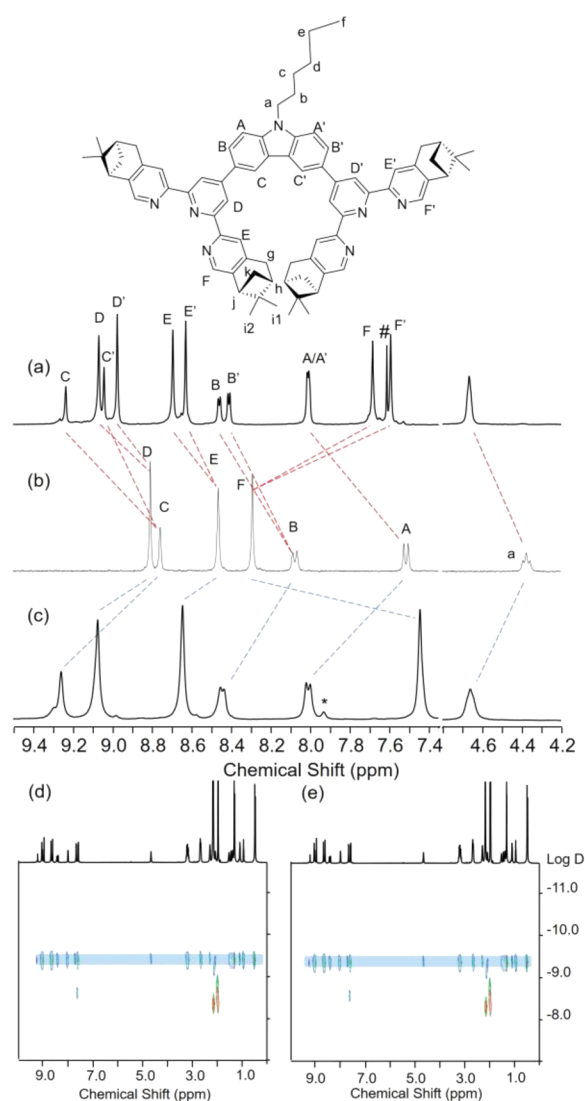


Figure 2. Partial ^1H NMR spectra (500 MHz) of (a) $[\text{Cd}_3\text{L}_3]$ in CD_3CN , (b) L in CDCl_3 , and (c) $[\text{Zn}_4\text{L}_4]$ in CD_3CN . # and * represent residue solvents (CHCl_3 and DMF). 2D DOSY NMR (500 MHz, CD_3CN , 300 K) for (d) $[\text{Cd}_3\text{L}_3]$ and (e) $[\text{Zn}_4\text{L}_4]$.

F and A'–F') probably because of the different chemical environments between the inner and outer rings caused by high strain in the trimeric macrocycle. All of the assignments shown in Figure 2 are readily confirmed by the 2D COSY and 2D NOESY spectra (Figures S7–S24). Furthermore, the diffusion-ordered NMR spectra (DOSY) of the $[\text{Cd}_3\text{L}_3]$ and $[\text{Zn}_4\text{L}_4]$ complexes display a narrow band at $\log D = -9.3$ and -9.4 , respectively (Figure 2d,e), suggesting the formation of discrete structures.

Additionally, electrospray ionization-mass spectrometry (ESI-MS) and traveling-wave ion mobility-mass spectrometry (TWIM-MS)²⁴ spectra were employed to provide further structural information for the expected assembly (Figure 3). ESI-MS of $[\text{Cd}_3\text{L}_3]$ displays a series of peaks with continuous charge states from 3+ to 6+ due to the loss of different numbers of PF_6^- counterions (Figure 3a; the deconvoluted mass is 4480 Da). The experimental isotope pattern of 5+ species is in accordance with the theoretical one of $([\text{Cd}_3\text{L}_3]\text{PF}_6)^{5+}$. In the TWIM-MS plots, each charge state ranging from 4+ to 6+ is observed with a narrow drift time

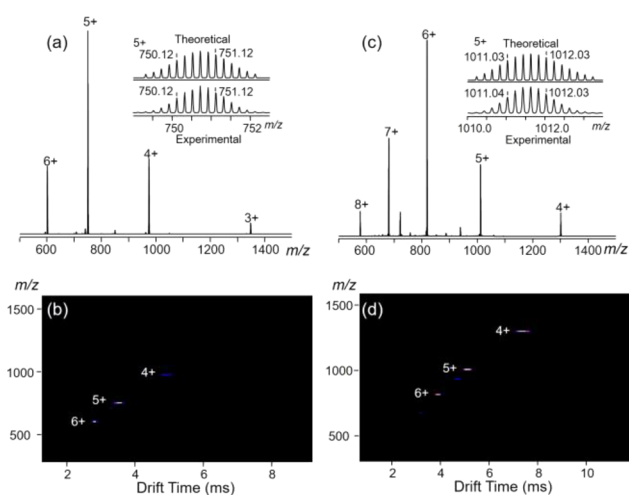


Figure 3. (a and c) ESI-MS and (b and d) TWIM-MS plots (m/z vs drift time) of $[\text{Cd}_3\text{L}_3]$ and $[\text{Zn}_4\text{L}_4]$. The insets of parts a and c show the theoretical and experimental isotope patterns of $[\text{Cd}_3\text{L}_3]^{5+}$ and $[\text{Zn}_4\text{L}_4]^{5+}$, respectively.

distribution, excluding the formation of other structural conformers or isomers (Figure 3b). Meanwhile, ESI-MS of $[\text{Zn}_4\text{L}_4]$ (Figure 3c) shows a dominate set of peaks with continuous charge states from 4+ to 8+, featured with well-resolved isotope patterns. The measured mass of $[\text{Zn}_4\text{L}_4]$ is 5778 Da, supporting its chemical composition. Narrowly distributed signals of each charge state in TWIM-MS (Figure 3d) suggest the formation of a rigid and shape-persistent structure.

We reasoned that the weaker coordination strength of cadmium(II) might introduce more flexibility and coordination deviation in the formation of a trimeric structure instead of a tetramer formed by zinc(II) because of the larger ionic radius of cadmium(II) (109 pm) than that of zinc(II) (88 pm).²⁵ Further evidence was provided by a molecular modeling study, and the results were summarized in Table S1. Distortions of the carbazole groups in the modeling structures of $[\text{Cd}_3\text{L}_3]^{6+}$ and $[\text{Zn}_3\text{L}_3]^{6+}$ were observed (shown in Figures 1c,d and S27–S29). In comparison, the four-membered-ring modeling structures ($[\text{Cd}_4\text{L}_4]^{8+}$ and $[\text{Zn}_4\text{L}_4]^{8+}$) did not display significant distortion via arrangement of the ligands in a herringbone way (Figures 1e,f and S26). Because of the distortion, the torsion energies per unit of $[\text{Cd}_3\text{L}_3]^{6+}$ and $[\text{Zn}_3\text{L}_3]^{6+}$ were much higher than those of $[\text{Cd}_4\text{L}_4]^{8+}$ and $[\text{Zn}_4\text{L}_4]^{8+}$ (Table S1). As a result, the lower torsion energy of $[\text{Zn}_4\text{L}_4]^{8+}$ contributed to its lower total energy per unit compared with $[\text{Zn}_3\text{L}_3]^{6+}$, suggesting that it is the enthalpically favorable structure. However, the selective formation of $[\text{Cd}_3\text{L}_3]^{6+}$ is determined by electrostatic repulsion, in which $[\text{Cd}_4\text{L}_4]^{8+}$ shows much higher electrostatic energy per unit.

To characterize the optical properties of **L** and the chiral metallomacrocycles, the UV–vis absorption spectra (Figure 4a) were collected first and analyzed with the help of theoretical calculation (Figure 4e). The calculation was performed based on density functional theory with 6-31G basis sets (see the details in the Supporting Information).²⁶ The experimental results were consistent well with the theoretical calculations with respect to the locations and relative intensities of the absorption peaks. In detail, **L** in Figure 4a shows a set of peaks at 264, 295, and 340 nm

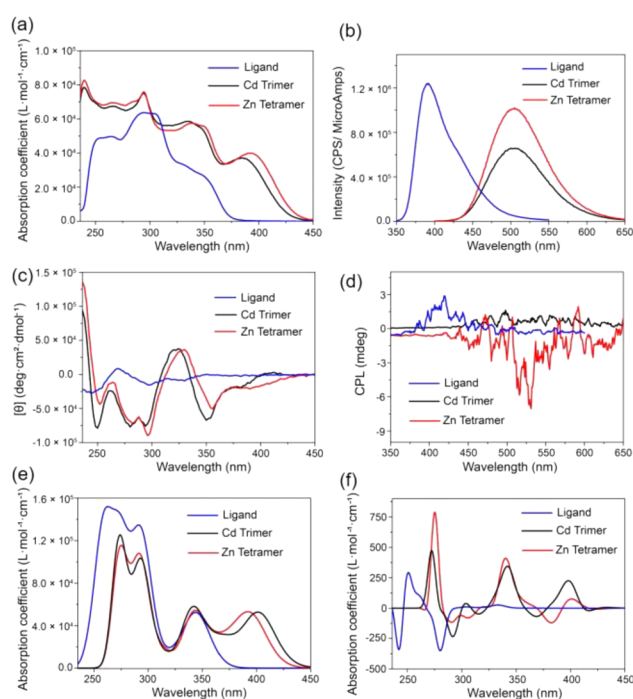


Figure 4. (a) UV–vis, (b) FL, (c) CD, and (d) CPL spectra and theoretical (e) UV–vis and (f) CD spectra of **L**, $[\text{Cd}_3\text{L}_3]$, and $[\text{Zn}_4\text{L}_4]$. Note: The absorption coefficient of **L** in part f was plotted at 20% of their actual values for an easier comparison. The concentrations of the repeating unit (**L**) in the solution of $[\text{Cd}_3\text{L}_3]$ and $[\text{Zn}_4\text{L}_4]$ were used to evaluate the corresponding absorption coefficient and $[\theta]$. The quantum yields of **L**, $[\text{Cd}_3\text{L}_3]$, and $[\text{Zn}_4\text{L}_4]$ were measured as 0.85, 0.43, and 0.65, respectively.

(shoulder), which refers to the electron transition (ET) from HOMO–7 to LUMO (local pyridinyl π – π^* transition), HOMO–1 to LUMO+1 (intramolecular charge transfer, ICT, from the carbazole to pyridinyl group), and HOMO to LUMO (π – π^* transition on the carbazole group), respectively (Figure S2). Upon complexation, a new peak centered at ca. 400 nm appears in both parts a and e of Figure 4 and is assigned to ET from HOMO to LUMO+12 (Figure S2; ligand-to-ligand charge transfer, LLCT).²⁷

In CD spectra (Figure 4c), **L** displays a weak positive Cotton effect (CE) at 268 nm. It indicates that only the pyridinyl rings attached to the chiral moieties are settled in some asymmetric environment, and no other long-ranged chiral induction exists because of the backbone flexibility. However, sophisticated CD signals on both spectra of $[\text{Cd}_3\text{L}_3]$ and $[\text{Zn}_4\text{L}_4]$ are observed, which show negative (ca. 380 nm), negative couplet (ca. 340 nm), and negative (ca. 295 nm) CEs. Among these rich and strong CEs, CEs at the LLCT (400 nm) absorption bands are characteristic and reveal that the chirality is transferred from chiral carbon centers to the coordination sites. Also, $[\text{Zn}_4\text{L}_4]$ with a more intense signal suggests that the chiral induction efficiency of the $[\text{Zn}_4\text{L}_4]$ macrocycle is higher than that of $[\text{Cd}_3\text{L}_3]$. The similar CD spectra of $[\text{Cd}_3\text{L}_3]$ and $[\text{Zn}_4\text{L}_4]$ suggest their similar chirality. Also, the calculated CD spectra based on the models of the complexes show signals similar to those of the experimental results (Figure 4f). In addition, the specific rotations of **L**, $[\text{Cd}_3\text{L}_3]$, and $[\text{Zn}_4\text{L}_4]$ were investigated. Both $[\text{Cd}_3\text{L}_3]$ ($[\alpha]_{\text{D}}^{25} = -135^\circ$; $c = 0.218$ in CH_3CN) and $[\text{Zn}_4\text{L}_4]$ ($[\alpha]_{\text{D}}^{25} = -131^\circ$; $c = 0.234$ in CH_3CN) revealed a larger negative specific rotation than that of **L**

($[\alpha]_D^{25} = -70^\circ$; $c = 0.220$ in CHCl_3), further suggesting chiral transmission from **L** to the macrocyclic backbone.

We then investigated the fluorescence (FL) properties of **L**, $[\text{Cd}_3\text{L}_3]$, and $[\text{Zn}_4\text{L}_4]$. As shown in Figure 4b, **L** emits light around 390 nm. After coordination, the light emission of $[\text{Cd}_3\text{L}_3]$ and $[\text{Zn}_4\text{L}_4]$ has an extraordinary red shift (~ 120 nm) to the green-light region (peaked at ca. 505 nm), which is assigned as a LLCT transition.^{7b} Compared with CD spectrometry, which characterizes the chiroptical property in the ground state, CPL spectrometry provides more chiral properties of the analytes in the excited state.^{7b} In addition, CPL has great potential application in photonic devices, such as 3D displays and energy-efficient backlights for LCD displays.²⁸ As a result, we investigated the CPL properties of **L**, $[\text{Cd}_3\text{L}_3]$, and $[\text{Zn}_4\text{L}_4]$. As shown in Figure 4d, **L** displays a positive CPL peak at ca. 400 nm. After coordination, $[\text{Zn}_4\text{L}_4]$ shows an obviously negative CPL peak at its emission region (centered at ca. 530 nm), which indicates that, in the excited state, the [tpy-Zn-tpy] luminophores are settled in a distinct chiral environment with that of the ligand. By comparison, $[\text{Cd}_3\text{L}_3]$ exhibits a much weaker positive CPL signal because of its lower quantum yield (Φ , 0.43) compared with Φ of **L** (0.85) and $[\text{Zn}_4\text{L}_4]$ (0.65). This also might be attributed to the combination of the positive signal from **L** and a much weaker negative signal from tpy-Cd^{II}. After deconvolution (the detailed method is summarized in the Supporting Information), the luminescence dissymmetry factors ($|g_{\text{lum}}|$),²⁹ which are used to evaluate the magnitude of CPL of **L**, $[\text{Cd}_3\text{L}_3]$, and $[\text{Zn}_4\text{L}_4]$ are around 8.8×10^{-4} ($\lambda_{\text{ex}} = 400$ nm), 4.0×10^{-4} ($\lambda_{\text{ex}} = 530$ nm), and 18.0×10^{-4} ($\lambda_{\text{ex}} = 530$ nm), respectively. The higher $|g_{\text{lum}}|$ of $[\text{Zn}_4\text{L}_4]$ indicates a higher efficiency in the chiral transmission and amplification from the ligand to metal center in the case of $[\text{Zn}_4\text{L}_4]$ than in $[\text{Cd}_3\text{L}_3]$. Notably, compared with the chiroptical properties of $[\text{Zn}_4\text{L}_4]$, the much weaker CPL signal of $[\text{Cd}_3\text{L}_3]$ is consistent with its weaker CE at the ICT absorption band in the ground state possibly because the larger ionic radius of cadmium(II) affected the chiral-transferring efficiency. These values are of the same order of magnitude as the values of other examples of biomacromolecules and chiral macromolecules.³⁰

In conclusion, we have successfully synthesized a new ditopic tcpy **L** by using 4'-bromo-substituted tcpy as the precursor. Such a ligand could coordinate with cadmium(II) and zinc(II) ions to form two chiral trimeric and tetrameric metallomacrocycles. The corresponding structures were confirmed by various techniques. Meanwhile, their optical properties were also investigated, exhibiting good CD and CPL response. This study represents a successful example of the tcpy framework in self-assembled macrocycles, thus advancing the complexity of tpy-based supramolecular systems. With 4'-bromo-substituted tcpy, we will be able to design and synthesize a series of multitopic chiral tpy ligands to assemble more sophisticated structures with the desired property and function.

■ ASSOCIATED CONTENT

● Supporting Information

The Supporting Information is available free of charge on the ACS Publications website at DOI: 10.1021/acs.inorgchem.9b02657.

General experimental methods, synthetic procedures, photophysical, electrochemical, self-assembly, and the-

oretical data, and ¹H and ¹³C NMR spectra for all new compounds (PDF)

■ AUTHOR INFORMATION

Corresponding Authors

*E-mail: xqhao@zzu.edu.cn (X.-Q.H.).

*E-mail: mpsong@zzu.edu.cn (M.-P.S.).

*E-mail: xiaopenglil@usf.edu (X.L.).

ORCID

Xinju Zhu: 0000-0003-1966-3480

Wenjing Zhang: 0000-0001-7964-6792

Ming Wang: 0000-0002-5332-0804

Xin-Qi Hao: 0000-0003-1942-8309

Mao-Ping Song: 0000-0003-3883-2622

Xiaopeng Li: 0000-0001-9655-9551

Notes

The authors declare no competing financial interest.

■ ACKNOWLEDGMENTS

We are grateful to the National Natural Science Foundation of China (Grants 21672192, 21803059, and 21929101), the China Postdoctoral Science Foundation (Grants 2016M602254 and 2016M600582), the Program for Science & Technology Innovation Talents in Universities of Henan Province (Grant 17HASTIT004), the Aid Project for the Leading Young Teachers in Henan Provincial Institutions (Grant 2015GGJS-157), and the Natural Science Foundation of Henan Province (Grant 182300410255).

■ REFERENCES

- (1) (a) Castilla, A. M.; Ramsay, W. J.; Nitschke, J. R. Stereochemistry in Subcomponent Self-Assembly. *Acc. Chem. Res.* **2014**, *47*, 2063–2073. (b) Liu, M.; Zhang, L.; Wang, T. Supramolecular Chirality in Self-Assembled Systems. *Chem. Rev.* **2015**, *115*, 7304–7397. (c) Chen, L.-J.; Yang, H.-B.; Shionoya, M. Chiral Metallosupramolecular Architectures. *Chem. Soc. Rev.* **2017**, *46*, 2555–2576.
- (2) (a) Fujita, M.; Tominaga, M.; Hori, A.; Therrien, B. Coordination Assemblies from a Pd(II)-Cornered Square Complex. *Acc. Chem. Res.* **2005**, *38*, 369–378. (b) Smulders, M. M.; Riddell, I. A.; Browne, C.; Nitschke, J. R. Building on Architectural Principles for Three-Dimensional Metallosupramolecular Construction. *Chem. Soc. Rev.* **2013**, *42*, 1728–1754. (c) Han, M.; Engelhard, D. M.; Clever, G. H. Self-Assembled Coordination Cages Based on Banana-Shaped Ligands. *Chem. Soc. Rev.* **2014**, *43*, 1848–1860. (d) Cook, T. R.; Stang, P. J. Recent Developments in the Preparation and Chemistry of Metallacycles and Metallacages via Coordination. *Chem. Rev.* **2015**, *115*, 7001–7045.
- (3) (a) Olenyuk, B.; Whiteford, J. A.; Fechtenkötter, A.; Stang, P. J. Self-assembly of Nanoscale Cuboctahedra by Coordination Chemistry. *Nature* **1999**, *398*, 796–799. (b) Chichak, K. S.; Cantrill, S. J.; Pease, A. R.; Chiu, S.-H.; Cave, G. W. V.; Atwood, J. L.; Stoddart, J. F. Molecular Borromean Rings. *Science* **2004**, *304*, 1308–1312. (c) Newkome, G. R.; Wang, P.; Moorefield, C. N.; Cho, T. J.; Mohapatra, P. P.; Li, S.; Hwang, S.-H.; Lukyanova, O.; Echegoyen, L.; Palagallo, J. A.; Iancu, V.; Hla, S.-W. Nanoassembly of a Fractal Polymer: A Molecular "Sierpinski Hexagonal Gasket". *Science* **2006**, *312*, 1782–1785. (d) Leigh, D. A.; Pritchard, R. G.; Stephens, A. J. A Star of David Catenane. *Nat. Chem.* **2014**, *6*, 978–982. (e) Wood, C. S.; Ronson, T. K.; Belenguer, A. M.; Holstein, J. J.; Nitschke, J. R. Two-Stage Directed Self-Assembly of a Cyclic [3]Catenane. *Nat. Chem.* **2015**, *7*, 354–358. (f) Fujita, D.; Ueda, Y.; Sato, S.; Mizuno, N.; Kumasaka, T.; Fujita, M. Self-Assembly of Tetravalent Goldberg Polyhedra from 144 Small Components. *Nature* **2016**, *540*, 563–566.

- (4) (a) Lee, S. J.; Lin, W. A Chiral Molecular Square with Metallo-Corners for Enantioselective Sensing. *J. Am. Chem. Soc.* **2002**, *124*, 4554–4555. (b) Ou-Yang, J.-K.; Zhang, Y.-Y.; He, M.-L.; Li, J.-T.; Li, X.; Zhao, X.-L.; Wang, C.-H.; Yu, Y.; Wang, D.-X.; Xu, L.; Yang, H.-B. Unexpected Self-Assembly of Chiral Triangles from 90° Chiral Di-Pt(II) Acceptors. *Org. Lett.* **2014**, *16*, 664–667. (c) Ye, Y.; Cook, T. R.; Wang, S.-P.; Wu, J.; Li, S.; Stang, P. J. Self-Assembly of Chiral Metallacycles and Metallacages from a Directionally Adaptable BINOL-Derived Donor. *J. Am. Chem. Soc.* **2015**, *137*, 11896–11899.
- (5) (a) Wild, A.; Winter, A.; Schlütter, F.; Schubert, U. S. Advances in the Field of π -Conjugated 2,2':6',2''-Terpyridines. *Chem. Soc. Rev.* **2011**, *40*, 1459–1511. (b) Schubert, U. S.; Winter, A.; Newkome, G. R. Synthesis, Properties, and Applications of Functionalized 2,2':6',2''-Terpyridines. *Terpyridine-Based Materials: For Catalytic, Optoelectronic and Life Science Applications*; Wiley-VCH Verlag GmbH & Co.: Weinheim, Germany, 2011.
- (6) (a) Winter, A.; Newkome, G. R.; Schubert, U. S. Catalytic Applications of Terpyridines and their Transition Metal Complexes. *ChemCatChem* **2011**, *3*, 1384–1406. (b) Sakamoto, R.; Wu, K.-H.; Matsuoka, R.; Maeda, H.; Nishihara, H. π -Conjugated Bis-(terpyridine)metal Complex Molecular Wires. *Chem. Soc. Rev.* **2015**, *44*, 7698–7714. (c) Chakraborty, S.; Newkome, G. R. Terpyridine-Based Metallocsupramolecular Constructs: Tailored Monomers to Precise 2D-Motifs and 3D-Metallo cages. *Chem. Soc. Rev.* **2018**, *47*, 3991–4016. (d) Wei, C.; He, Y.; Shi, X.; Song, Z. Terpyridine-Metal Complexes: Applications in Catalysis and Supramolecular Chemistry. *Coord. Chem. Rev.* **2019**, *385*, 1–19.
- (7) (a) Hofmeier, H.; Hoogenboom, R.; Wouters, M. E. L.; Schubert, U. S. High Molecular Weight Supramolecular Polymers Containing Both Terpyridine Metal Complexes and Ureidopyrimidinone Quadruple Hydrogen-Bonding Units in the Main Chain. *J. Am. Chem. Soc.* **2005**, *127*, 2913–2921. (b) Tsukamoto, T.; Takada, K.; Sakamoto, R.; Matsuoka, R.; Toyoda, R.; Maeda, H.; Yagi, T.; Nishikawa, M.; Shinjo, N.; Amano, S.; Iokawa, T.; Ishibashi, N.; Oi, T.; Kanayama, K.; Kinugawa, R.; Koda, Y.; Komura, T.; Nakajima, S.; Fukuyama, R.; Fuse, N.; Mizui, M.; Miyasaki, M.; Yamashita, Y.; Yamada, K.; Zhang, W.; Han, R.; Liu, W.; Tsubomura, T.; Nishihara, H. Coordination Nanosheets Based on Terpyridine–Zinc(II) Complexes: As Photoactive Host Materials. *J. Am. Chem. Soc.* **2017**, *139*, 5359–5366. (c) Zheng, Z.; Opilik, L.; Schiffmann, F.; Liu, W.; Bergamini, G.; Ceroni, P.; Lee, L.-T.; Schütz, A.; Sakamoto, J.; Zenobi, R.; VandeVondele, J.; Schlüter, A. D. Synthesis of Two-Dimensional Analogues of Copolymers by Site-to-Site Transmetalation of Organometallic Monolayer Sheets. *J. Am. Chem. Soc.* **2014**, *136*, 6103–6110. (d) He, T.; Gao, Y.; Chen, R.; Ma, L.; Rajwar, D.; Wang, Y.; Grimsdale, A. C.; Sun, H. Multiphoton Harvesting in an Angular Carbazole-Containing Zn(II)-Coordinated Random Copolymer Mediated by Twisted Intramolecular Charge Transfer State. *Macromolecules* **2014**, *47*, 1316–1324.
- (8) (a) Wang, J.-L.; Li, X.; Lu, X.; Hsieh, I. F.; Cao, Y.; Moorefield, C. N.; Wesdemiotis, C.; Cheng, S. Z. D.; Newkome, G. R. Stoichiometric Self-Assembly of Shape-Persistent 2D Complexes: A Facile Route to a Symmetric Supramacromolecular Spoked Wheel. *J. Am. Chem. Soc.* **2011**, *133*, 11450. (b) Chakraborty, S.; Hong, W.; Endres, K. J.; Xie, T. Z.; Wojtas, L.; Moorefield, C. N.; Wesdemiotis, C.; Newkome, G. R. Terpyridine-Based, Flexible Tripods: From a Highly Symmetric Nanosphere to Temperature-Dependent, Irreversible, 3D Isomeric Macromolecular Nanocages. *J. Am. Chem. Soc.* **2017**, *139*, 3012–3020. (c) Schmittel, M.; Kalsani, V.; Kishore, R. S. K.; Cölfen, H.; Bats, J. W. Dynamic and Fluorescent Nanoscale Phenanthroline/Terpyridine Zinc(II) Ladders. Self-Recognition in Unlike Ligand/Like Metal Coordination Scenarios. *J. Am. Chem. Soc.* **2005**, *127*, 11544–11545. (d) Mittal, N.; Pramanik, S.; Paul, I.; De, S.; Schmittel, M. Networking Nanoswitches for ON/OFF Control of Catalysis. *J. Am. Chem. Soc.* **2017**, *139*, 4270–4273. (e) Chen, M.; Wang, J.; Liu, D.; Jiang, Z.; Liu, Q.; Wu, T.; Liu, H.; Yu, W.; Yan, J.; Wang, P. Highly Stable Spherical Metallo-Capsule from a Branched Hexapodal Terpyridine and Its Self-Assembled Berry-type Nanostructure. *J. Am. Chem. Soc.* **2018**, *140*, 2555–2561. (f) Chen, M.; Wang, J.; Wang, S.-C.; Jiang, Z.; Liu, D.; Liu, Q.; Zhao, H.; Yan, J.; Chan, Y.-T.; Wang, P. Truncated Sierpiński Triangular Assembly from a Molecular Mortise–Tenon Joint. *J. Am. Chem. Soc.* **2018**, *140*, 12168–12174. (g) Chan, Y.-T.; Li, X.; Soler, M.; Wang, J.-L.; Wesdemiotis, C.; Newkome, G. R. Self-Assembly and Traveling Wave Ion Mobility Mass Spectrometry Analysis of Hexacadmium Macrocycles. *J. Am. Chem. Soc.* **2009**, *131* (45), 16395–16397. (h) Fu, J.-H.; Lee, Y.-H.; He, Y.-J.; Chan, Y.-T. Facile Self-Assembly of Metallo-Supramolecular Ring-in-Ring and Spiderweb Structures Using Multivalent Terpyridine Ligands. *Angew. Chem., Int. Ed.* **2015**, *54*, 6231–6235. (i) Wang, S.-Y.; Fu, J.-H.; Liang, Y.-P.; He, Y.-J.; Chen, Y.-S.; Chan, Y.-T. Metallo-Supramolecular Self-Assembly of a Multi-component Ditrigon Based on Complementary Terpyridine Ligand Pairing. *J. Am. Chem. Soc.* **2016**, *138*, 3651–3654. (j) Gao, Y.; He, T.; Hu, P.; Koh, T. M.; Sun, H.; Grimsdale, A. C. Influence of H-Bonding on Self-Assembly and Tunable Dual-Emission of Carbazole-Based Zn(II)-Terpyridine Metallo-cycles. *Macromol. Chem. Phys.* **2014**, *215*, 753–762.
- (9) Elmas, S.; Beelders, W.; Bradley, S. J.; Kroon, R.; Laufersky, G.; Andersson, M.; Nann, T. Platinum Terpyridine Metallopolymer Electrode as Cost-Effective Replacement for Bulk Platinum Catalysts in Oxygen Reduction Reaction and Hydrogen Evolution Reaction. *ACS Sustainable Chem. Eng.* **2017**, *5*, 10206–10214.
- (10) (a) Sun, W.; Parowatkin, M.; Steffen, W.; Butt, H.-J.; Mailänder, V.; Wu, S. Ruthenium-Containing Block Copolymer Assemblies: Red-Light-Responsive Metallopolymers with Tunable Nanostructures for Enhanced Cellular Uptake and Anticancer Phototherapy. *Adv. Healthcare Mater.* **2016**, *5*, 467–473. (b) Wang, H.; Qian, X.; Wang, K.; Su, M.; Haoyang, W.-W.; Jiang, X.; Brzozowski, R.; Wang, M.; Gao, X.; Li, Y.; Xu, B.; Eswara, P.; Hao, X.-Q.; Gong, W.; Hou, J.-L.; Cai, J.; Li, X. Supramolecular Kandinsky circles with high antibacterial activity. *Nat. Commun.* **2018**, *9*, 1815.
- (11) (a) Chen, P.; Li, Q.; Grindy, S.; Holten-Andersen, N. White-Light-Emitting Lanthanide Metallo-gels with Tunable Luminescence and Reversible Stimuli-Responsive Properties. *J. Am. Chem. Soc.* **2015**, *137*, 11590–11593. (b) Yin, G.-Q.; Wang, H.; Wang, X.-Q.; Song, B.; Chen, L.-J.; Wang, L.; Hao, X.-Q.; Yang, H.-B.; Li, X. Self-Assembly of Emissive Supramolecular Rosettes with Increasing Complexity Using Multitopic Terpyridine Ligands. *Nat. Commun.* **2018**, *9*, 567.
- (12) (a) Kröhnke, F. The Specific Synthesis of Pyridines and Oligopyridines. *Synthesis* **1976**, *1976*, 1–24. (b) Newkome, G. R.; Hager, D. C.; Kiefer, G. E. Chemistry of Heterocyclic Compounds. Part 119. Synthesis of Halogenated Terpyridines and Incorporation of the Terpyridine Nucleus into a Polyetheral Macrocyclic. *J. Org. Chem.* **1986**, *51*, 850–853. (c) Jameson, D. L.; Guise, L. E. An Improved, Two-Step Synthesis of 2,2':6',2''-terpyridine. *Tetrahedron Lett.* **1991**, *32*, 1999–2002.
- (13) (a) Dehaut, J.; Husson, J.; Guyard, L. A More Efficient Synthesis of 4,4',4''-Tricarboxy-2,2':6',2''-terpyridine. *Green Chem.* **2011**, *13*, 3337–3340. (b) Duric, S.; Sypaseuth, F. D.; Hoof, S.; Svensson, E.; Tzschucke, C. C. Synthesis of Asymmetrically Substituted Terpyridines by Palladium-Catalyzed Direct C-H Arylation of Pyridine N-Oxides. *Chem. - Eur. J.* **2013**, *19*, 17456–17463. (c) Robo, M. T.; Prinsell, M. R.; Weix, D. J. 4,4',4''-Trimethyl-2,2':6',2''-terpyridine by Oxidative Coupling of 4-Picoline. *J. Org. Chem.* **2014**, *79*, 10624–10628.
- (14) (a) Heller, M.; Schubert, U. S. Syntheses of Functionalized 2,2':6',2''-Terpyridines. *Eur. J. Org. Chem.* **2003**, *2003*, 947–961. (b) Fallahpour, R.-A. Synthesis of 4'-Substituted-2,2':6',2''-Terpyridines. *Synthesis* **2003**, *2*, 155–184.
- (15) Hayoz, P.; von Zelewsky, A. New Versatile Optically Active Bipyridines as Building Blocks for Helicating and Caging Ligands. *Tetrahedron Lett.* **1992**, *33*, 5165–5168.
- (16) (a) Chelucci, G.; Thummel, R. P. Chiral 2,2'-Bipyridines, 1,10-Phenanthrolines, and 2,2':6',2''-Terpyridines: Syntheses and Applications in Asymmetric Homogeneous Catalysis. *Chem. Rev.* **2002**, *102*, 3129–3170. (b) Mamula, O.; von Zelewsky, A. Supramolecular Coordination Compounds with Chiral Pyridine and Polypyridine Ligands Derived from Terpenes. *Coord. Chem. Rev.* **2003**, *242*, 87–95.

- (17) (a) Ziegler, M.; Monney, V.; Stoeckli-Evans, H.; von Zelewsky, A.; Sasaki, I.; Dupic, G.; Daran, J.-C.; Balavoine, G. G. A. Complexes of New Chiral Terpyridyl Ligands. Synthesis and Characterization of Their Ruthenium(II) and Rhodium(III) Complexes. *J. Chem. Soc., Dalton Trans.* **1999**, 667–675. (b) Malkov, A. V.; Baxendale, I. R.; Bella, M.; Langer, V.; Fawcett, J.; Russell, D. R.; Mansfield, D. J.; Valko, M.; Kočovský, P. Synthesis of New Chiral 2,2'-Bipyridyl-Type Ligands, Their Coordination to Molybdenum(0), Copper(II), and Palladium(II), and Application in Asymmetric Allylic Substitution, Allylic Oxidation, and Cyclopropanation. *Organometallics* **2001**, *20*, 673–690.
- (18) (a) Zheng, Y.; Harms, K.; Zhang, L.; Meggers, E. Enantioselective Alkynylation of 2-Trifluoroacetyl Imidazoles Catalyzed by Bis-Cyclometalated Rhodium(III) Complexes Containing Pinene-Derived Ligands. *Chem. - Eur. J.* **2016**, *22*, 11977–11981. (b) Gong, J.; Wan, Q.; Kang, Q. Gold(I)/Chiral Rh(III) Lewis Acid Relay Catalysis Enables Asymmetric Synthesis of Spiroketal and Spiroaminals. *Adv. Synth. Catal.* **2018**, *360*, 4031–4036.
- (19) (a) Zhang, X.-P.; Mei, J.-F.; Lai, J.-C.; Li, C.-H.; You, X.-Z. Mechano-Induced Luminescent and Chiroptical Switching in Chiral Cyclometalated Platinum(II) Complexes. *J. Mater. Chem. C* **2015**, *3*, 2350–2357. (b) Li, X.-L.; Hu, M.; Yin, Z.; Zhu, C.; Liu, C.-M.; Xiao, H.-P.; Fang, S. Enhanced Single-Ion Magnetic and Ferroelectric Properties of Mononuclear Dy(III) Enantiomeric Pairs through the Coordination Role of Chiral Ligands. *Chem. Commun.* **2017**, *53*, 3998–4001. (c) Wan, Q.; Xiao, X.-S.; To, W.-P.; Lu, W.; Chen, Y.; Low, K.-H.; Che, C.-M. Counteranion- and Solvent-Mediated Chirality Transfer in the Supramolecular Polymerization of Luminescent Platinum(II) Complexes. *Angew. Chem., Int. Ed.* **2018**, *57*, 17189–17193.
- (20) (a) Yan, J.; Wang, Y.-B.; Zhu, Z.-H.; Li, Y.; Zhu, X.; Hao, X.-Q.; Song, M.-P. Synthesis, Characterization, and Catalytic Studies of Unsymmetrical Chiral NCC Pincer Pd(II) and Ni(II) Complexes Bearing (Imidazolyl)aryl NHC Ligands. *Organometallics* **2018**, *37*, 2325–2334. (b) Zhu, Z.-H.; Li, Y.; Wang, Y.-B.; Lan, Z.-G.; Zhu, X.; Hao, X.-Q.; Song, M.-P. α -Alkylation of Nitriles with Alcohols Catalyzed by NNN' Pincer Ru(II) Complexes Bearing Bipyridyl Imidazoline Ligands. *Organometallics* **2019**, *38*, 2156–2166. (c) Liu, J.-K.; Gong, J.-F.; Song, M.-P. Chiral Palladium Pincer Complexes for Asymmetric Catalytic Reactions. *Org. Biomol. Chem.* **2019**, *17*, 6069–6098.
- (21) (a) Wang, M.; Wang, C.; Hao, X.-Q.; Li, X.; Vaughn, T. J.; Zhang, Y.-Y.; Yu, Y.; Li, Z.-Y.; Song, M.-P.; Yang, H.-B.; Li, X. From Trigonal Bipyramidal to Platonic Solids: Self-Assembly and Self-Sorting Study of Terpyridine-Based 3D Architectures. *J. Am. Chem. Soc.* **2014**, *136*, 10499–10507. (b) Wang, L.; Liu, R.; Gu, J.; Song, B.; Wang, H.; Jiang, X.; Zhang, K.; Han, X.; Hao, X.-Q.; Bai, S.; Wang, M.; Li, X.; Xu, B.; Li, X. Self-Assembly of Supramolecular Fractals from Generation 1 to 5. *J. Am. Chem. Soc.* **2018**, *140*, 14087–14096.
- (22) Ivchenko, P. V.; Nifant'ev, I. E.; Buslov, I. V. A Convenient Approach for the Synthesis of 2,6-Diformyl- and 2,6-diacetylpyridines. *Tetrahedron Lett.* **2013**, *54*, 217–219.
- (23) (a) Bernhard, S.; Takada, K.; Díaz, D. J.; Abruña, H. D.; Mürner, H. Enantiomerically Pure Chiral Coordination Polymers: Synthesis, Spectroscopy, and Electrochemistry in Solution and on Surfaces. *J. Am. Chem. Soc.* **2001**, *123*, 10265–10271. (b) Barron, J. A.; Glazier, S.; Bernhard, S.; Takada, K.; Houston, P. L.; Abruña, H. D. Photophysics and Redox Behavior of Chiral Transition Metal Polymers. *Inorg. Chem.* **2003**, *42*, 1448–1455.
- (24) (a) Brocker, E. R.; Anderson, S. E.; Northrop, B. H.; Stang, P. J.; Bowers, M. T. Structures of Metallosupramolecular Coordination Assemblies Can Be Obtained by Ion Mobility Spectrometry–Mass Spectrometry. *J. Am. Chem. Soc.* **2010**, *132*, 13486–13494. (b) Li, X.; Chan, Y.-T.; Newkome, G. R.; Wesdemiotis, C. Gradient Tandem Mass Spectrometry Interfaced with Ion Mobility Separation for the Characterization of Supramolecular Architectures. *Anal. Chem.* **2011**, *83*, 1284–1290.
- (25) Meier, M. A. R.; Lohmeijer, B. G. G.; Schubert, U. S. Relative Binding Strength of Terpyridine Model Complexes under Matrix-Assisted Laser Desorption/Ionization Mass Spectrometry Conditions. *J. Mass Spectrom.* **2003**, *38*, 510–516.
- (26) (a) Kohn, W.; Sham, L. J. Self-Consistent Equations Including Exchange and Correlation Effects. *Phys. Rev.* **1965**, *140*, A1133–A1138. (b) Kohn, W. Nobel Lecture: Electronic Structure of Matter—Wave Functions and Density Functionals. *Rev. Mod. Phys.* **1999**, *71*, 1253–1266.
- (27) Tang, Y.; Kong, M.; Tian, X.; Wang, J.; Xie, Q.; Wang, A.; Zhang, Q.; Zhou, H.; Wu, J.; Tian, Y. A Series of Terpyridine-Based Zinc(II) Complexes Assembled for Third-Order Nonlinear Optical Responses in the Near-Infrared Region and Recognizing Lipid Membranes. *J. Mater. Chem. B* **2017**, *5*, 6348–6355.
- (28) Yang, Y.; da Costa, R. C.; Smilgies, D.-M.; Campbell, A. J.; Fuchter, M. J. Induction of Circularly Polarized Electroluminescence from an Achiral Light-Emitting Polymer via a Chiral Small-Molecule Dopant. *Adv. Mater.* **2013**, *25*, 2624–2628.
- (29) Riehl, J. P.; Richardson, F. S. Circularly Polarized Luminescence Spectroscopy. *Chem. Rev.* **1986**, *86*, 1–16.
- (30) (a) Shen, C.; Anger, E.; Srebro, M.; Vanthuyne, N.; Deol, K. K.; Jefferson, T. D.; Muller, G.; Williams, J. A. G.; Toupet, L.; Roussel, C.; Autschbach, J.; Réau, R.; Crassous, J. Straightforward Access to Mono- and Bis-Cycloplatinated Helicenes Displaying Circularly Polarized Phosphorescence by Using Crystallization Resolution Methods. *Chem. Sci.* **2014**, *5*, 1915–1927. (b) Cheng, J.; Hao, J.; Liu, H.; Li, J.; Li, J.; Zhu, X.; Lin, X.; Wang, K.; He, T. Optically Active CdSe-Dot/CdS-Rod Nanocrystals with Induced Chirality and Circularly Polarized Luminescence. *ACS Nano* **2018**, *12*, 5341–5350.